Optics and Laser Technology 103 (2018) 219–225

Contents lists available at ScienceDirect

Optics and Laser Technology

journal homepage: www.elsevier.com/locate/optlastec

Full length article

Multi-PSF fusion in image restoration of range-gated systems

Canjin Wang [a,*], Tao Sun [a], Tingfeng Wang [a], Xikui Miao [b], Rui Wang [a]

[a] State Key Laboratory of Laser Interaction with Matter, Changchun Institute of Optics, Fine Mechanics and Physics, Chinese Academy of Science, Changchun, Jilin, China
[b] Key Laboratory of Electro-optical Countermeasures Test & Evaluation Technology, Luo Yang, Henan, China

ARTICLE INFO

Article history:
Received 14 August 2017
Received in revised form 3 December 2017
Accepted 9 January 2018

Keywords:
Range-gated imaging
Image restoration
PSF fusion
Backscattering
Iterative optimization

ABSTRACT

For the task of image restoration, an accurate estimation of degrading PSF/kernel is the premise of recovering a visually superior image. The imaging process of range-gated imaging system in atmosphere associates with lots of factors, such as back scattering, background radiation, diffraction limit and the vibration of the platform. On one hand, due to the difficulty of constructing models for all factors, the kernels from physical-model based methods are not strictly accurate and practical. On the other hand, there are few strong edges in images, which brings significant errors to most of image-feature-based methods. Since different methods focus on different formation factors of the kernel, their results often complement each other. Therefore, we propose an approach which combines physical model with image features. With an fusion strategy using GCRF (Gaussian Conditional Random Fields) framework, we get a final kernel which is closer to the actual one. Aiming at the problem that ground-truth image is difficult to obtain, we then propose a semi data-driven fusion method in which different data sets are used to train fusion parameters. Finally, a semi blind restoration strategy based on EM (Expectation Maximization) and RL (Richardson-Lucy) algorithm is proposed. Our methods not only models how the lasers transfer in the atmosphere and imaging in the ICCD (Intensified CCD) plane, but also quantifies other unknown degraded factors using image-based methods, revealing how multiple kernel elements interact with each other. The experimental results demonstrate that our method achieves better performance than state-of-the-art restoration approaches.

1. Introduction

Range-gated imaging system has a wide range of applications in conditions lack of illumination, such as imaging and monitoring at night, remote surveillance and so on. Due to relative motions, backscattering, speckle noise and many other adverse factors, the image is seriously degraded, which leads to inevitable information loss. Updating hardware may be the most direct way to improve the performance of imaging system, while also maybe expensive. Another feasible way is to use image restoration technology to recover sharp images from the collected degraded images.

Image restoration is an important and challenging research topic. Although lots of techniques have been proposed to deal with this problem, they cannot be directly applied to range-gated imaging system due to the difficulty of estimating the PSF (Point Spread Function) of the system. Our research focuses on this topic. Shan et al. [1]'s work indicates that the more accurate the kernel is estimated, the better current restoration methods perform. Therefore, a more explicit handling of degraded PSF estimation error is critical for better restoration results. Once we get an accurate PSF, we can recover an sharp image by non-blind deconvolution methods, which are relatively mature.

Over the past decades, remarkable research efforts have been devoted to developing degraded kernel estimation methods. Cho and Lee [2] predict strong image structures from an estimated latent image, and use them instead of gray values to formulate the optimization function. With GPU implementation facilitates, their method is fast enough for practical application. Cho et al. [3] propose an approach to estimate the Random Transform of the degraded kernel using edges of the blurry image, and get the degraded kernel by Inverse Random Transform. In Fergus et al. [4]'s approach, a manual-specified process is required to supply an image region without saturation effects, and the kernel is estimated using a prior on image gradients in a coarse-to-fine framework. In this framework, the spatial domain prior on natural images leads to a capability to handle seriously blurred image. Instead of performing a MAP (Maximum A Posteriori) estimation, Goldstein and Fattal [5] try to estimate the power spectrum of the degraded kernel by a power-law of the natural image along with an spectral whitening formula, then recover the kernel by a phase retrieval method. Pan et al. [6] develop a L0-regularized

* Corresponding author.
E-mail address: wangcanjin@ciomp.ac.cn (C. Wang).

https://doi.org/10.1016/j.optlastec.2018.01.038
0030-3992/

intensity based method to obtain salient properties of the degraded image without any complex filtering strategies or additional selection processes, and use them to obtain a reliable degraded kernel. Shan et al. [1] introduce a unified probabilistic model which contains several novel terms of image prior. While each approach above has achieved significant success in their particular experiment dataset, none of them can get satisfying result in all cases. For our application, these approaches still have following defects:

(1) Most approaches are designed to deal with motion blur by camera shake, while image degradation in our range gated imaging system contains many other factors.
(2) A large part of these algorithms are based on strong edges, which may be difficult to extract in low-light condition.
(3) The priors for natural image are not suitable for illumination image.

Therefore, the existing PSF estimation method cannot be directly applied in our system. The PSFs estimated by different approaches sometimes differ widely, as they incorporate different priors in each individual frameworks. The bad news is that it's difficult to determine which one is optimal and there does not exist a generic solution for all degraded images. Mai and Liu [7] address that the PSFs from different approaches often complement each other and with a proper fusing strategy, combining multiple PSFs may lead to a more accurate one. Inspired by their work, we are eager to know whether making use of different priors of the system with appropriate merging strategies may bring an outstanding result. The answer is yes.

The basic clue in our approach is to merge various individual PSFs into a more accurate one. We construct an imaging model and make use of imaging procedure instead of images to obtain a SPSF (system-based PSF). Then by using state-of-art kernel estimation methods based on different image features, we get some FeaPSFs (feature-based PSFs). These PSFs respectively contain different part of features in the imaging system, which are complementary and redundant with each other. With a fusion strategy based on GCRF framework, we joint these individual efforts into mutual work and get a final FuPSF (fusion PSF).

We develop a semi-data-driven training method using RTF (Regression Tree Field) framework to train the fusion parameters. The probability distribution models of inlier and outlier pixels are established. With EM and RL method we iteratively estimate latent image and update the FuPSF.

2. Imaging model

In range-gated imaging system, illumination and echo beam may be disturbed by factors such as atmospheric attenuation, background radiation and atmospheric aerosol backscattering, which dramatically degrade the performance of system. The model of range-gated image system is shown in Fig. 1.

Considering the factors in laser beam propagation path, the imaging model of the system is established to estimate SPSF. In gate opening time, factors affecting the imaging quality involve those following parts: target reflection, scattering, background radiation, speckle, atmospheric turbulence, diffraction limit and so on. Some factors carry the target information, while others cover the target information [8,9].

2.1. Reflected energy

Reflected energy is the part of laser energy that reaches the camera imaging surface through outbound atmospheric transmission, target reflection and inbound atmospheric transmission, which can be expressed as:

$$P_r = P_t \frac{A_\Delta}{R^2 \Omega_l} \frac{A_r}{R^2} T_a^2(R) \eta_t \eta_r \tag{1}$$

where P_r donates reflected energy, P_t donates emitting energy, η_t donates the efficiency of emitting system, η_r donates the efficiency of receiving system, A_r donates the entrance pupil area of the receiving optical system, A_Δ donates effective covered area on target, Ω_l donates solid angle of laser beam.

2.2. Backscatter energy

The forward transmission light is scattered by the atmosphere, and a part of it enters the observation system against the optical axis, which masks the true image information, resulting in a decrease in contrast and resolution. This phenomenon is called backscattering, which is related to factors such as atmospheric scattering coefficient, scattering angle distribution, the distance between receiving optical system and laser, the divergence angle and the FOV (Field of Vision) of the optical system.

Let l_o donate the distance between imaging system and the intersection of laser divergence angle and optical system angle, l_m donate imaging distance, E_p donate single pulse laser energy, then the backscattered energy can be expressed as:

$$E_{backscatter} = E_p \eta_t \eta_r A_r \frac{\sigma_e}{8\pi} \int_{l_o}^{l_m} \frac{\exp(-2\sigma_e l)}{l^2} dl \tag{2}$$

2.3. Background radiant energy

Background radiation energy means the energy of natural radiation light entering the optical system. In the gating opening time, the background radiation energy E_b can be calculated as:

$$E_b = \frac{\rho_b}{\pi} L_\lambda \Delta\lambda \eta_r \Omega_r A_r \Delta\tau \tag{3}$$

where L_λ donates background spectral radiation, $\Delta\lambda$ donates the bandwidth of the receiving optical system (which can be regarded as a bandpass filter), ρ_b donates the average reflection coefficient of the background, $\Delta\tau$ donates single opening time of camera.

2.4. MTF of the atmospheric transmission

Since reflected and forward-scattered light contain useful target information, while back-scattered light overwhelms the information, we define the MTF (Modulation Transfer Function) of the atmospheric transmission as:

$$MTF_{atmosphere} = \frac{\pi}{4} F\left(\frac{E_d + E_f}{E_d + E_f + E_b}\right) \tag{4}$$

2.5. Diffraction limit

Due to the optical system aperture limitation, the diffraction limit of the imaging system [10] needs to be considered as a factor of image degradation. The MTF of diffraction is calculated as:

$$MTF_{diffraction} = \frac{2}{\pi}\left[\arccos\frac{f}{f_{co}} - \frac{f}{f_{co}}\sqrt{1-\left(\frac{f}{f_{co}}\right)^2}\right], \quad 0 < f < f_{co} \tag{5}$$

where f donates the spatial frequency, and f_{co} donates the cutoff frequency of the imaging plane.

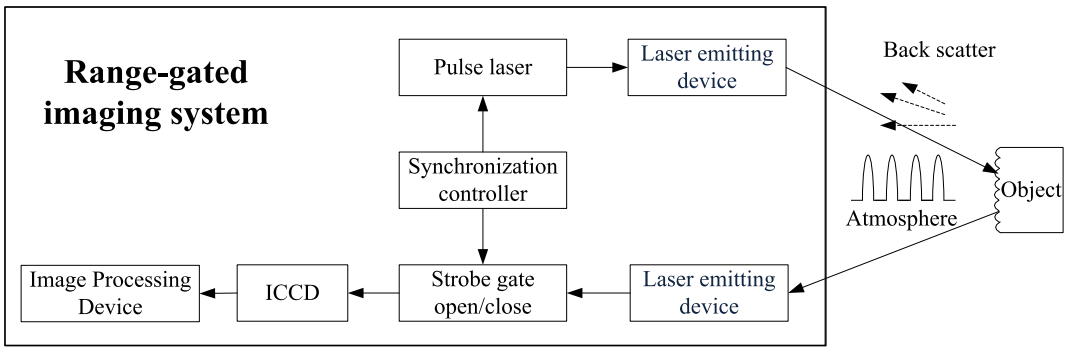

Fig. 1. Model of range-gated imaging system.

2.6. Sensor distortion

The projection of the object on the camera plane is distorted, which is mainly determined by the pixel size. The MTF is expressed as:

$$MTF_{distorted} = \frac{\sin(\pi f d_p)}{\pi f d_p} \tag{6}$$

where f and d_p donates the spatial frequency and the pixel size of the camera, respectively.

3. PSF estimation

3.1. SPSF estimation

Considering the degraded factors described in Section 2, the MTF of the imaging system can be calculated as:

$$SMTF = MTF_{atmosphere} \cdot MTF_{diffraction} \cdot MTF_{distorted} \tag{7}$$

Due to the circular symmetry of the optical device, the SPSF of the system can be calculated by one-dimensional integral [11], which is described as:

$$SPSF(\theta) = 2\pi \int J_0(2\pi\theta f_s) MTF(f_s) f_s df_s \tag{8}$$

where J_0 donates the Bessel function, f_s donates the spatial frequency in cycles per radian, and θ donates the offset with respect to the optical axis.

3.2. FeaPSF estimation

In recent years lots of restoration frameworks have been proposed which are mostly based on image features. Here we simply list some state-of-the-art works. Cai et al. [12] use a tight-wavelet framework to regularize the sparsity of blur kernel and improve the Split-Bregman method to solve the energy function without any prior information. GoldStein et al. [5] present a model based on a natural-image-power law, which better accounts for biases arising from large and strong edge. Combine the model with a whitening spectrum formula, the spectrum distribution of the kernel can be estimated. Tai et al. [13] propose an iterative framework in which the estimated camera motion is used to constrain the noise features of the image. Cho et al. [2] use strong edges predicted from the estimated latent image with derivatives to formulate the optimization function. Fergus et al. [4] use an manually-specified image region without saturation effects to estimate the blur kernel, then construct a joint posterior probability function between the latent and degraded image.

In this article we make use of some of state-of-art approaches [1,2,4,5,13] with our system-based strategy to obtain a fused kernel, then we will compare the performance of our approach with each single method.

4. Multi-PSF fusion

In [7] Mai and Liu demonstrated that fusing multiple kernels from different methods may outperform each individual one. They developed a data-driven method based on GCRF which can effectively learn a good kernel fusion model from abundant training images. In their approach, the model parameters are updated by minimizing an energy function:

$$P(k|\{k_i\}) \propto \exp(-E(k|\{k_i\})) \tag{9}$$

$$E(k|\{k_i\}) = \sum_{p\in k} E_u(k(p)|\{k_i(p)\}) + \sum_{p\in k, q\in N(p)} E_s(k(p),k(q)|\{k_i(p),k_i(q)\}) \tag{10}$$

where k_i donates the individual kernel obtained by ith estimation method, k donates the fused kernel, E donates the energy function composed of two energy terms E_u and E_s, E_u donates local energy at each node, E_s donates local energy at each pair of neighboring nodes, $N(p)$ donates nodes neighboring to p.

Unfortunately, in our imaging system neither latent images nor ground-truth kernels are available, which makes the training process impossible to implement. To deal with this problem, we develop a semi-data-based training method to determine different parameters separately. Our training process is based on the framework of EM algorithm and separated into two steps: updating the parameters of FeaPSF and updating the parameters of SPSF.

4.1. Updating the coefficients of FeaPSF

In this step we fix SPSF as a constant. Considering the fact that FeaPSF is only concerned with image characteristics, we acquire non-active-imaging images in low light condition which is similar in imaging characteristics as training data. These images can be considered as images from active illumination after removing the PSFPM effects. In this step with the absence of other factors, we can approximately treat them as the ground truth image. We blur each image with eight different kernels which are shown in Fig. 2 and used GCRF framework to train the fusion weight, just as mentioned in Mai and Liu [7]'s approach.

4.2. Updating the coefficient of SPSF

According to formula (8), the expression of SPSF contains some system related parameters. In this case, its fusion parameter should also be dynamic [14]. We model the parameter as a function of imaging distance L and the single pulse energy of laser E_p.

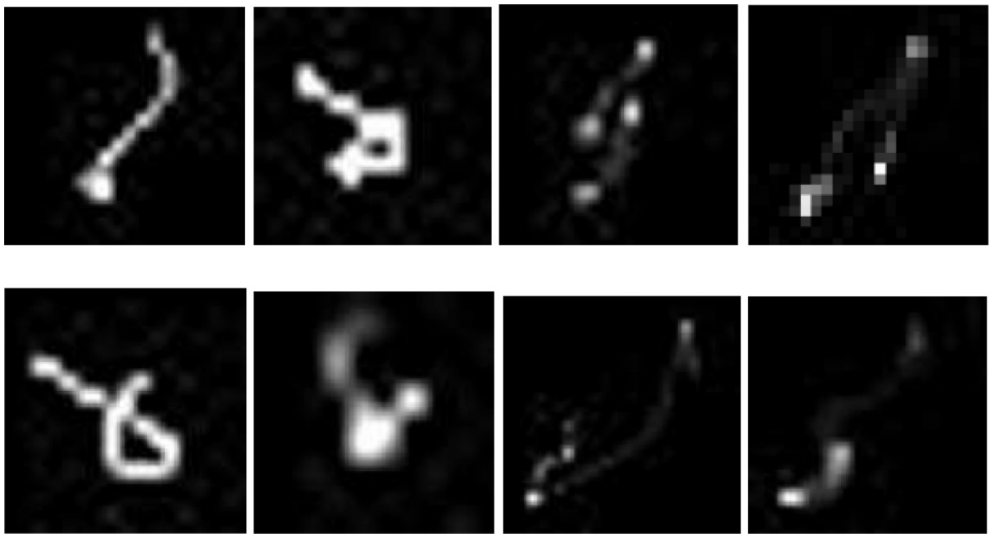

Fig. 2. Kernels used to generate synthetically blurred dataset.

We fix the coefficients of FeaPSF, and select different targets at different distances (100 m–1 km) with a step length of 50 m. The laser pulse power changes from 5 mJ to 50 mJ with a step length of 1 mJ, at each step the range gated images are collected. We adopt the x-step in [15] to get deblur image:

$$f_F(F) = \sum_{D_*} \omega_* ||KD_*F - D_*G|| + l_1||D_hF||^2 + l_1||D_vF||^2 + \frac{l_2}{|M|}\sum_{i\in M}\rho(P_iF - q^i) + \gamma\sum_{i\in M}(\sigma^i - F_{ref}^{-1}(F_{\sigma,x}(\sigma^i)))^2 \quad (11)$$

where K, G and F respectively represent the degraded kernel, degraded image and latent image, D_* donates partial derivative operator in different directions, ω_* donates the corresponding weight of D_*, D_h are the first order differentiation operators along the horizontal axes and D_v the vertical. P_i donates an operator which extracts a patch at location i in latent image F, Z_i is a vector representing the example patch assigned to location i, q_i is defined as $q_i = \sigma_i Z_i + \mu_i$. By optimizing $f_F(F)$ we can get the estimation of latent image F.

The best fusion coefficient of SPSF is determined according to the following formula

$$\hat{\omega}_{sPSF}(l, Ep) = \max_{\hat{F}}(LC(\hat{F})) \quad (12)$$

where $LC(\cdot)$ represents local contrast operator. The restored image with maximal LC value is considered to be with best image quality, which means that, the fusion PSF is closest to the real one. After finding the corresponding $\hat{\omega}_{sPSF}(l, Ep)$ at different l and E_p, a nonlinear regression process is needed to determine the parameters α_p and α_l according to formula (13).

$$\omega_{sPSF} = \frac{\alpha_p E_p \exp(-\alpha_l l)}{l^2} \quad (13)$$

5. Deconvolution

Image deconvolution is a severely ill-posed problem, a small deviation of PSF may lead to a large decline in image quality [16]. In this case we proposed an iterative semi blind-deconvolution strategy. Firstly we take system model and image features into account and execute the fusion strategy described above to estimate a coarse PSF, and use it as the initial value of the iteration. During the recovery, the PSF and recovered image are updated alternately. Since the semi blind-restoration is more specific than blind restoration, it can generally achieve better restoration result.

Since the images in our system contain lots of outliers such as the saturated pixels, light veins [17] and speckle noise, deconvolution without proper outliers handling may bring severe ringing artifacts. We combine the *EM* method with *RL* deconvolution. The deconvolution is considered as a MAP estimation problem. In E-step, we compute the weights of each pixels as:

$$W^t = \frac{\mathbf{P}(G|K*F)P_i}{\mathbf{P}(G|K*F)P_i + \mathbf{Ga}(G|K*F)(1-P_i)} \quad (14)$$

where $\boldsymbol{P}(G|K*F)$ is a Poisson distribution, $\boldsymbol{Ga}(G|K*F)$ is a Gaussian distribution, $P_i(x)$ is the probability that pixel x belongs to the inliers. The way to calculate P_i refers to Cho et al. [2].

In M-step, the latent image is updated as:

$$F^{t+1} = \frac{F^t}{1 + (|\partial_h F^t|^\alpha + |\partial_v F^t|^\alpha)} \cdot K \otimes \left(\frac{G \cdot W^t}{F^t * K} + 1 - W^t\right) \quad (15)$$

where α is a constant. Once we get the updated latent image, the PSF can also be corrected by their cooperation. Instead of using intensity values, we update K in the gradient space:

$$k^{t+1} = \min_k(||\nabla f * k - \nabla g||_2^2 + \gamma||k||_2^2) \quad (16)$$

The computation of formula (16) is mainly consisted of FFTs and can be executed efficiently. The negative elements of K_{t+1} is set to 0.

6. Computer simulation results

We implement our approach in MATLAB and conduct experiments on a PC with 3.4 GHZ Core i7 CPU and 16 GB RAM. We established two datasets consist of a large amount of images. Dataset A is composed of low light images with variety of scene content from real life and online sources, including Flickr, Facebook, and Google Plus. These images span a wide variety of scene content such as natural scenes, buildings, indoor objects and so on. Dataset B is composed of images with changing lighting parameters from our range-gated imaging system. We change the laser power, imaging distance, and the solid angle of laser beam and capture a series of pictures. Then we select eight kernels from [7], which are shown in Fig. 2, implement them to dataset A to generate our synthetically

blurred image dataset. For each blurred image in dataset A, we have got its ground-truth image and blur kernel, so that we can use them to train the fusion coefficients of FeaPSFs and test the performance of the restoration methods. To make use of dataset B, we changing ω_{sPSF} in Section 4 to regress the best fusion coefficient of SPSF. In each iteration we randomly select 100 images from dataset A and B as the train sets, and 10 images from datasets B as the test set, and calculate the average results.

We compare our approach with the state-of-art methods [1,2,4,5,13]. Once a method fails in one blurred image (due to the program crash), the image is discarded, so that each valid image should have 6 estimated PSFs including the fusion one.

6.1. Fusion performance

Firstly we evaluate the effectiveness of our fusion method to find out whether it performs better than other single-kernel methods in dataset A. All the parameters for state-of-the-art methods are kept as the authors suggest in the implementations. To determine the precision and the mean of the local Gaussian model, we adopt the RTF framework. In dataset A, the ground-truth image is easy to get. So that we use the average MAE (mean absolute error) between each estimated kernel and ground-truth kernel to evaluate the kernel estimation accuracy of the methods. Also we evaluate the recover performance according to the visual quality of the restored image by different kernels using two metrics [18,19]: PSNR (the peak-signal-to-noise ratio) and SSIM (the structure similarity index). PSNR and SSIM directly measure the gray-level and structure similarity between the reconstruction results and ground-truth images. The average results are shown in Table 1.

It can be observed that the PSFs from our proposed method are the most similar to the ground-truth PSF, which indicates that the fusion strategy effectively combine different PSF features, thus represents the actual degradation process more closely. Also the highest PSNR and SSIM indicate that our proposed fusion method supplies better kernel estimation than other individual methods, which leads to visually better deconvolution results.

6.2. Restoration results in range-gated imaging system

6.2.1. Restoration results

In this step we use our method to deal with images from real range-gated imaging systems, to check if the method works for real images. As the ground truth images are impossible to obtain, we choose Information Capacity(IC) [15] as the metric of the restoration methods, which is defined as:

$$C_{\inf o}(d,\theta) = \log_2\left\{1 + \sum_{w}\frac{\log[p(i,j,d,\theta)]}{\log[\max(p(i,j,d,\theta))]}\right\} \tag{17}$$

where $i, j = 1, 2, \ldots, L$ is the gray level, d and θ donates the distance and angle between pixels. While d and θ is determined, $p(i,j)$ is called gray co-occurrence matrix. w donates restrain area in matrix p. In images with higher quality, the distribution of frequence has larger density in the area besides $i = j$, which leads to higher C_{info}. That's why we use IC to measure the image quality with no reference images. In this article, we choose $d = 1$ and $\theta = 0°$, 45° and 90°, so C_{info} is described as:

$$C_{\inf\ o} = \alpha C_{\inf\ o}(1,0°) + \beta C_{\inf\ o}(1,45°) + \gamma C_{\inf\ o}(1,90°) \tag{18}$$

where α, β, γ are constant and $\alpha + \beta + \gamma = 1$.

We select a white number on the wall at distance of 2.5 km and a tower at distance of 3.0 km as our observation target. Illuminate them with laser beam and the images are cropped to 150×150 pixels, which are shown in Fig. 3. We compared our approach with state-of-art restoration methods. The results are shown in Figs. 4 (a)–(f), 5(a)–(f) and Table 2.

In range-gated imaging system the image quality changes with laser power. Typically, larger laser energy leads to higher image quality while the camera is not overexposed. In order to verify the adaptability of our algorithm, the laser power ranges from 10 mJ to 40 mJ and the restoration results are evaluated, as is shown in Fig. 6.

6.2.2. Discussion

As is shown in Figs. 4(a) and 5(a), the restoration results by Fergus [4] are not satisfactory with severe over-smoothing, which may be ascribed to the error of the gradient distribution model in condition of low light and severe noise. Figs. 4(b) and 5(b) illustrate that due to the imposed contrast constraint in fuzzy parts, the restoration results by Shan [1] are with severe ringing artifacts. In Cho [2], as is shown in Figs. 4(c) and 5(c), the ringing artifacts are effectively suppressed, but the results suffer from inaccurate edge estimation, which leads to fuzzy edge. Because of the extremely high sensitivity of noise, in Goldstein [5] the results suffer from both severe ringing artifacts and fuzzy edges, as is shown in Figs. 4 (d) and 5(d). In Tai [13]'s results, each iteration is divided into two steps consisted of denoising and kernel estimation, better kernel estimation leads to fewer ringing artifacts, but fuzzy edges still exist, as is shown in Figs. 5(e) and 6(e). Comparatively speaking, our approach provide a more accurate kernel which fuses system-based kernel with image-feature-based kernels, and the restoration results are with fewer ringing artifacts, better details and higher contrast. From Table 2 we can draw the same conclusion, the *IC* values of our method are higher than others, which means that our restoration results are with better image quality.

From Fig. 6 we can observe that the image qualities from all approaches increase as the laser power increases. Randomly sampled in the cross coordinates, the results of our algorithm are the best, which proves that our algorithm has good environment adaptability.

Table 1
Average PSNR and SSIM of different restoration methods. The best performance is shown in bold.

Method	MAE ($\times 10^{-3}$)	PSNR	SSIM
Fergus [4]	8.03	21.45	0.623
Shan [1]	4.75	24.18	0.726
Cho [2]	4.92	23.67	0.701
Goldstein [5]	5.84	23.25	0.748
Tai [13]	3.84	25.75	0.802
Our's	**3.25**	**27.13**	**0.869**

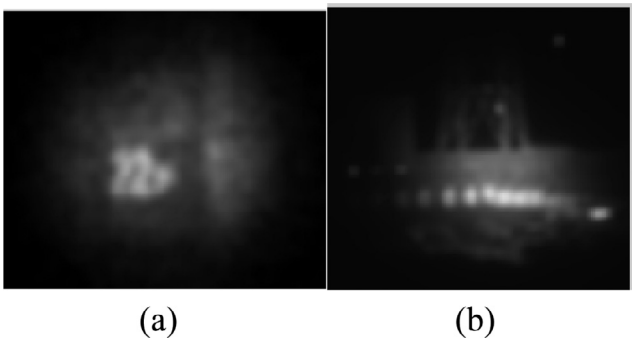

Fig. 3. Degraded image of (a) number at distance of 2.5 km and (b) tower at distance of 3.0 km. Scenes in illustrated area are blurred and noisy with unsatisfactory visual effects.

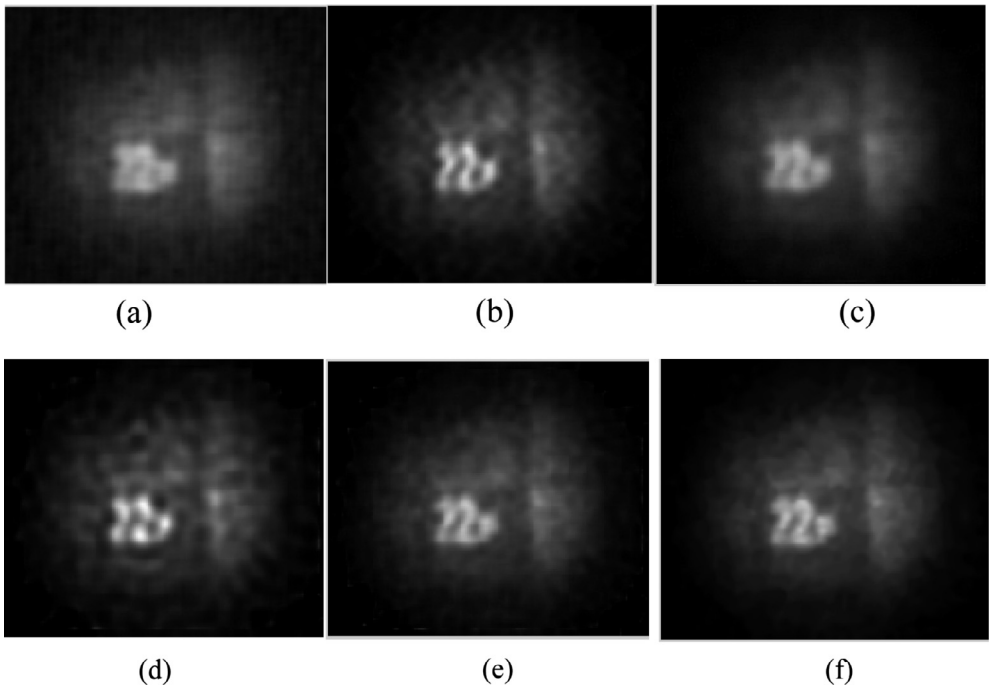

Fig. 4. Restored results of number picture by (a) Fergus's method, (b) Shan's method, (c) Cho's method, (d) Goldstein's method, (e) Tai's method and (f) proposed method.

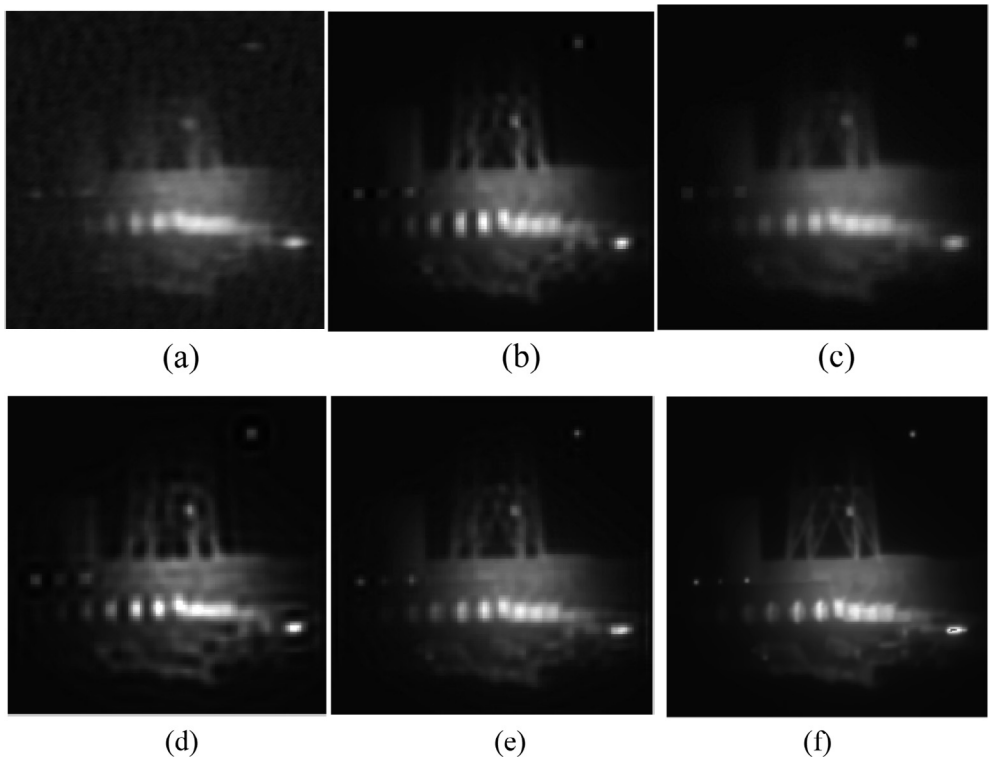

Fig. 5. Restored results of tower picture by (a) Fergus's method, (b) Shan's method, (c) Cho's method, (d) Goldstein's method, (e) Tai's method and (f) proposed method.

Table 2
IC values of restored results. The best performance is shown in bold.

	Degraded image	Fergus's	Shan's	Cho's	Goldstein's	Tai's	Our's
Number	0.3458	0.4925	0.6715	0.5218	0.6256	0.7615	**0.8125**
Tower	0.4172	0.4832	0.7136	0.5417	0.7534	0.8132	**0.8972**

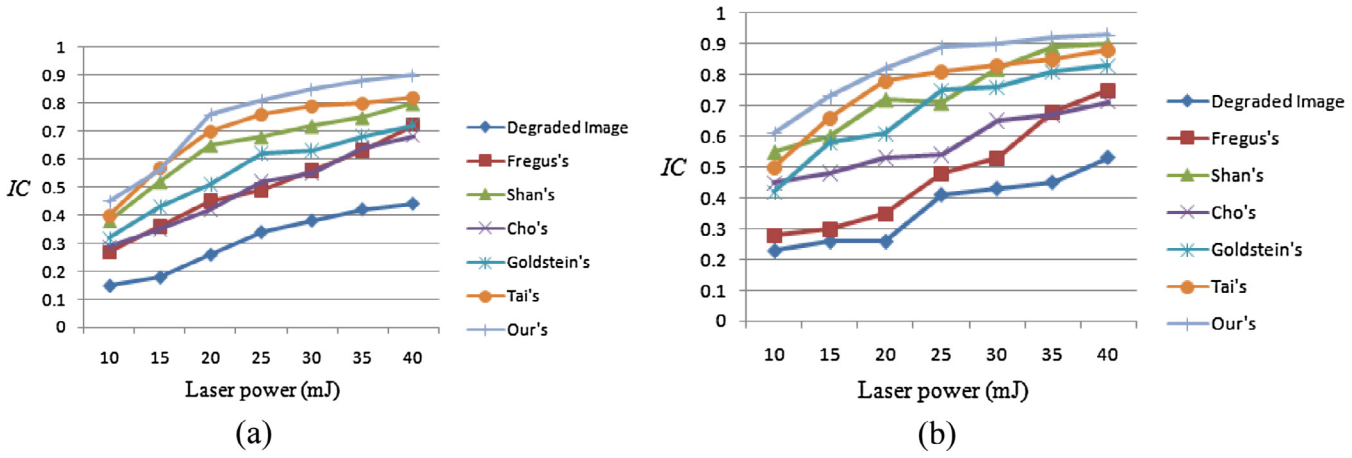

Fig. 6. *IC* values of (a) number (b) tower pictures in different laser power. Our approach outperforms others regardless of laser power.

7. Conclusion

Range-gated imaging system is a challenging situation for image restoration. Due to low contrast, high noise and fuzzy edges, traditional edge/gradient-based restoration methods cannot achieve satisfactory performance. In this article, a new kernel estimation method based on fusion strategy is proposed. We model the imaging procedure to calculate a SPSF, and then get some FeaPSFs by using state-of-art kernel estimation methods based on different image features. These kernel are fused into a final FuPSF based on GCRF framework. Then a semi-data-driven training method using RTF framework is used to train the fusion parameters. The experimental results indicate that our method provide a more accurate kernel, which results in better restoration quality. By changing some model parameters, the proposed algorithm can also be extended to underwater laser imaging system.

Acknowledgements

This paper is supported by Opening Foundation of Key Laboratory of Electro-optical Countermeasures Test & Evaluation Technology GKCP2016004. The authors would like to thank the reviewers for their valuable comments and suggestions that improve the presentation of this paper.

References

[1] Q. Shan, J. Jia, A. Agarwala, High-quality motion deblurring from a single image, ACM Trans. Graph. 27 (2008) 73.
[2] S. Cho, S. Lee, Fast motion deblurring, ACM Trans. Graph. 28 (2009) 145–152.
[3] T.S. Cho, S. Paris, B.K.P. Horn, W.T. Freeman, Blur kernel estimation using the radon transform, in: Proceedings of the IEEE Conference on Computer Vision and Pattern Recognition (CVPR), Colorado Springs, USA, 2011, pp. 241–248.
[4] R. Fergus, B. Singh, A. Hertzmann, S.T. Roweis, W.T. Freeman, Removing camera shake from a single photograph, ACM Trans. Graph. 25 (2006) 787–794.
[5] A. Goldstein, R. Fattal, Blur-kernel estimation from spectral irregularities, in: European Conference on Computer Vision, Firenze, Italy, 2012, pp. 622–635.
[6] J. Pan, Z. Hu, Z. Su, M.H. Yang, Deblurring text images via l0-regularized intensity and gradient prior, in: Proceedings of the IEEE Conference on Computer Vision and Pattern Recognition (CVPR), Columbus, USA, 2014, pp. 2901–2908.
[7] L. Mai, F. Liu, Kernel fusion for better image deblurring, in: Proceedings of the IEEE Conference on Computer Vision and Pattern Recognition (CVPR), Boston, USA, 2015, pp. 371–380.
[8] C. Vannahme, M. Dufva, A. Kristensen, High frame rate multi-resonance imaging refractometry with distributed feedback dye laser sensor, Light Sci. Appl. 4 (2015) e269.
[9] N. Meitav, E.N. Ribak, S. Shoham, Point spread function estimation from projected speckle illumination, Light Sci. Appl. 5 (2016) e16048.
[10] J.L. Wu, Y.Q. Xu, J.J. Xu, X.M. Wei, A.C. Chan, A.H. Tang, et al., Ultrafast laser-scanning time-stretch imaging at visible wavelengths, Light Sci. Appl. 6 (2017) 6.
[11] W. Hou, D.J. Gray, A.D. Weidemann, G.R. Fournier, J.L.Forand, Automated underwater image restoration and retrieval of related optical properties, in: IEEE International Geoscience and Remote Sensing Symposium, Barcelona, Spain, 2007, pp. 1889–1892.
[12] J.F. Cai, H. Ji, C.Q. Liu, Z.W. Shen, Framelet based blind motion deblurring from a single image, IEEE Trans. Image Process. 21 (2) (2012) 562–572.
[13] Y.W. Tai, S. Lin, Motion-aware noise filtering for deblurring of noisy and blurry images, in: Proceedings of the Computer Vision and Pattern Recognition (CVPR), Providence, Rhode Island, 2012, pp. 17–24.
[14] C.P.T. McPolin, N. Olivier, J.S. Bouillard, D. O'connor, A.V. Krasavin, W. Dickson, et al., Universal switching of plasmonic signals using optical resonator modes, Light Sci. Appl. 6(6) (2017).
[15] L. Sun, S. Cho, J. Wang, J. Hays, Edge-based blur kernel estimation using patch priors, in: Proceedings of the IEEE International Conference on Computational Photography (ICCP), Cambridge, USA, 2013, pp. 1–8.
[16] A. Levin, Y. Weiss, F. Durand, W.T. Freeman, Understanding blind deconvolution algorithms, IEEE Trans. Pattern Anal. Mach. Intell. 33 (12) (2011) 2354–2367.
[17] C.J. Wang, T. Sun, T.F. Wang, R. Wang, J. Guo, Y.Z. Tian, Model-based restoration using light vein for range-gated imaging systems, Appl. Opt. 55 (26) (2016) 7229–7235.
[18] S. Cho, J. Wang, S. Lee, Handling outliers in non-blind image deconvolution, in: Proceedings of the IEEE International Conference on Computer Vision (ICCV), Barcelona, Spain, 2011, pp. 495–502.
[19] H. Han, X. Zhang, W. Ge, Performance evaluation of underwater range-gated viewing based on image quality metric, in: 9th International Conference on Electronic Measurement & Instruments, Beijing, China, 2009, pp. 4-441–4-444.